# Coupling Through Tortuous Path Narrow Slot Apertures into Complex Cavities

Russell P. Jedlicka, *Senior Member, IEEE*, Steven P. Castillo, *Senior Member, IEEE*, and Larry K. Warne

*Abstract*—A hybrid finite-element method/method of moments (FEM/MOM) model has been implemented to compute the coupling of fields into a cavity through narrow slot apertures having depth. The model utilizes the slot model of Warne and Chen [24]–[30], which takes into account the depth of the slot, wall losses, and dielectrics with air gaps in the slot region. The cavity interior is modeled with the mixed-order covariant-projection elements of Crowley [33]. Results are given showing the accuracy and generality of the method for modeling geometrically complex slot-cavity combinations.

*Index Terms*—Boundary integral equations, electromagnetic interference, finite-element methods, method of moments.

## I. INTRODUCTION

ELECTROMAGNETIC coupling can adversely impact a multitude of applications ranging from modern telecommunication systems to sophisticated electronic warfare equipment. The primary coupling issues are electromagnetic compatibility and interference, either intentional or unintentional. The functionality of the systems involved, which typically consist of numerous subsystems operating concurrently, can be characterized in terms of their susceptibility, vulnerability, and survivability in the electromagnetic environment in which they are expected to operate.

To design effectively hardened, complex operational systems, it is critical to characterize the worst case electromagnetic coupling, that is, the upper bound of the field penetrating a system and the distribution of the energy within that complicated system. System performance may be compromised by a variety of penetration mechanisms. In this study, it is assumed that the shield is constructed from good electrical conductors so diffusion can be ignored and isolated so conductive effects are negligible. Back-door coupling occurs through inadvertent cracks and gaps created by warping or bowing at the mechanical interfaces between pieces of a shielded enclosure. These back-door phenomena are much less predictable or controllable and so merit particular interest and study.

R. P. Jedlicka and S. P. Castillo are with the Klipsch School of Electrical and Computer Engineering, New Mexico State University, Las Cruces, NM 88003 USA.

L. K. Warne is with the Sandia National Laboratories, Albuquerque, NM 87185 USA.
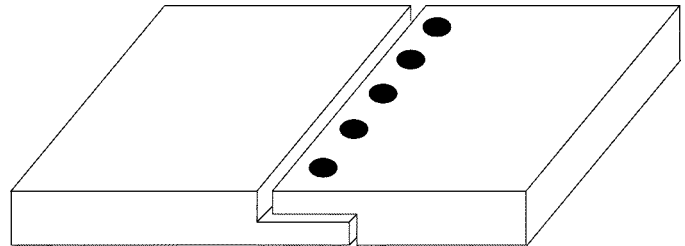
Fig. 1.   Bolted seam.

Coupling through unforeseen apertures such as the tortuous-path lapped seam, depicted in Fig. 1, into conducting cavities is the major thrust of this work. To model realistic coupling problems, it is necessary to develop a model which includes a three-dimensional (3-D) representation of the slot/cavity configuration. Specifically, such a model should incorporate narrow slot apertures having depth, loss, and gaskets backed by arbitrarily shaped cavities filled with inhomogeneous lossy dielectrics. The model should also incorporate the effect of the finite conductivity of the enclosure walls.

The conceptual formulation for the cavity-backed aperture has been presented in detail by Harrington and Mautz [1] as well as Butler *et al.* [2]. The generalized network formulation presentation in the former is an extension of the work published by Harrington [3]. In both papers, the problem is segmented into an interior and an exterior region. Equivalent problems are formulated for the two regions and coupled through the boundary conditions in the aperture. In these formulations, the interior and exterior are generally considered to be homogeneous and, except for the aperture, the regions are isolated by good electric conductors. Wang *et al.* considered not only transmission into, but also scattering from, conducting bodies with arbitrary apertures [4]. In this work, they formulated the 3-D problem for arbitrarily shaped bodies and apertures; however, only zero thickness slots were considered. In addition, the interior region did not include inhomogeneous media since an integral equation method was used.

In 1988, Taflove *et al.* applied a finite-difference time-domain (FDTD) technique to the analysis of narrow slots and lapped joints in a two-dimensional conducting screen [5]. This paper recognized the importance of narrow slot apertures, in particular, the tortuous paths associated with lapped joints.

Following the work of Merewether [6], Riley and Turner applied the FDTD technique to the analysis of a cavity-backed aperture loaded by boxes and terminated wires. Their hybrid thin-slot algorithm [7] advances the earlier work of Gilbert and Holland [8]. Later in 1990, they incorporated the model of Warne and Chen into an FDTD analysis of a narrow slot
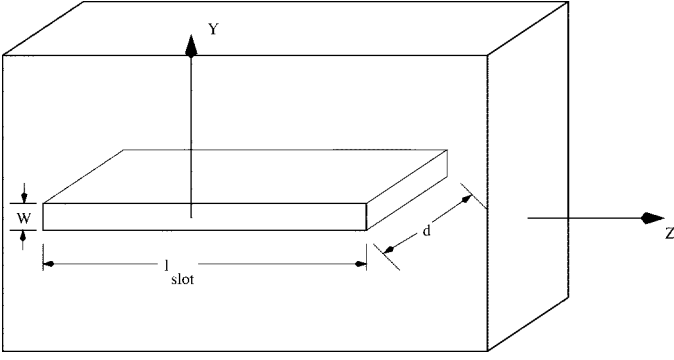
Fig. 2.  Narrow-slot aperture with depth.



Fig. 3.  Local cross section of slot.

aperture having depth and losses into a regularly shaped cavity [9].

The demand for solutions of aperture/cavity problems has brought progress in numerical techniques and their application. Historically, finite-difference techniques have received greater attention in electromagnetics; the use of the finite-element method (FEM) has been more recent. Subsequently, hybrid techniques using boundary integral/modal expansion techniques, method of moments (MOM)/FDTD methods as well as finite-element/boundary integral formulations have become commonplace [11]–[21]. Nonzero thickness was incorporated by using finite-difference techniques or FEM to solve the interior problem increasing the computational size of the problem considerably. In recent years, the FEM has proven to be a useful electromagnetic compatibility (EMC) prediction tool [22], [23].

The research performed to date demonstrates the maturity of hybrid numerical methods in electromagnetics. The only slot/cavity work that incorporated a practical slot model was the effort of Riley and Turner [7]. In a more recent paper, their finite-difference implementation was modified to accommodate curved surfaces; however, neither wall loss nor dielectric inhomogeneities were included [10]. Thus, another formulation and solution are required to include additional features in the model of a real world system.

In this paper, we present a hybrid numerical technique which can be used to calculate the amount of energy penetrating a system through a narrow slot aperture with depth and, at the same time, to determine its disposition; that is, of the power available in an impinging wave, how much is lost during transmission through the aperture and dissipated in the walls and dielectrics occupying the interior, and how much is delivered to loads, or components, within the configuration. Specifically, this involves computing the electromagnetic coupling through narrow slot apertures into complex cavities (arbitrarily shaped, with an inhomogeneous dielectric loading). The slot models of Warne and Chen [24]–[30] are coupled to a 3-D vector FEM formulation for the interior cavity region. Warne and Chen's slot model avoids the need to resolve a tortuous path slot with a very fine finite-element or finite-difference mesh while being general enough to include dielectrics in the slot interior, slot wall losses, and bolt loading across the slot [31]. In addition, the slot model can be extended to include very deep slots in which a resonance is excited in the depth direction. A comparison is made
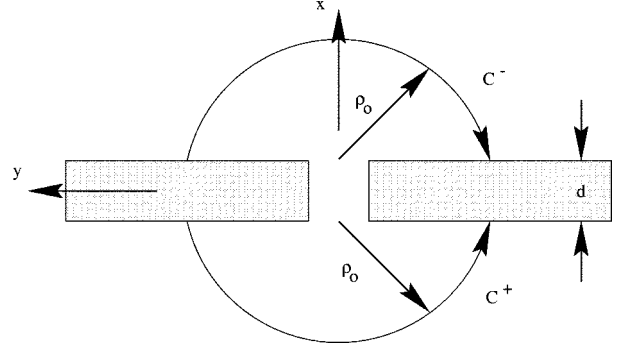
between experimental and numerical results for several different slot-cavity combinations to validate the model.

## II. COUPLED SLOT-CAVITY MODEL

Consider the slot geometry in Fig. 2. The depth through the slot may be a tortuous path more characteristic of overlapped joints. Warne and Chen's model assumes that

$$l_{\text{slot}}, \lambda \gg \rho_o \gg d. \tag{1}$$

The slot walls are assumed to have a large but finite conductivity so that they can be characterized by the usual perturbation

$$Z_s = R_s + jX_s = \sqrt{\frac{j\omega\mu}{\sigma + j\omega\epsilon}} \approx (1+j)\sqrt{\frac{\omega\mu}{2\sigma}}. \tag{2}$$

Consider Fig. 3. The governing integro-differential equation, as a function of the magnetic current along the slot, is given as

$$H_z^-(\rho_o^-, z) + \frac{1}{4Z_{\rho_o}} \frac{d^2 I_m}{dz^2} - Y_{\rho_o} \frac{I_m}{4} = -\frac{H_z^{SC}(z)}{2}$$
$$= -H_z^{\text{inc}}(z) \tag{3}$$

where

$$H_z^-(\rho_o^-, z)$$
$$= \left[ \left( \frac{-j}{\omega\mu_o} \right) \left( \frac{d^2}{dz^2} + k^2 \right) \right] \int_{-h}^{h} I_m(z') \frac{e^{-jkR_o}}{4\pi R_o} dz' \tag{4}$$

and

$$R_o = \sqrt{\rho_o^2 + (z - z')^2}. \tag{5}$$

The half length of the slot is $h$, and $\rho_o$ is the radial distance on the illuminated side. The transmission-line coefficient terms are

$$Z_{\rho_o} = Z_{\text{int}} + j\omega L_{\rho_o}$$
$$Z_{\text{int}} = R + j\omega L_{\text{int}} \tag{6}$$

$$Y_{\rho_o} = G + j\omega C_{\rho_o}. \tag{7}$$

The parameters $L_{\rho_o}$ and $C_{\rho_o}$ are the per-unit-length transmission-line parameters for the slot with lossless walls and no gasket. The parameters $R$, $L_{\text{int}}$, and $G$ represent the per-unit-length transmission-line parameters for the slot when

the walls are lossy and a lossy gasket material is contained in the slot. Note that (3)–(7) are dependent on the radial distance $\rho_o$ which is arbitrary.

Using the equivalent antenna radius derived by Warne and Chen [25], [26] and assuming that the field in the unilluminated region $H_z^-$ is in an infinite half-space, the slot equations evaluated at $\rho_o = a$ become

$$H_z^-(a, z) + \frac{\Delta Y_L}{4} \frac{d^2 I_m(z)}{dz^2} - \frac{\Delta Y_C}{4} I_m(z) = -H_z^{\text{inc}}(z) \quad (8)$$

where

$$H_z^-(a, z) = \left[ \left( \frac{-j}{\omega \mu_o} \right) \left( \frac{d^2}{dz^2} + k^2 \right) \right] \int_{-h}^{h} I_m(z') \frac{e^{-jkR_a}}{4\pi R_a} dz' \quad (9)$$

and

$$\Delta Y_C = G + j\omega C_{\rho_o} - j\omega C_{\rho_o}^o \quad (10)$$

$$\Delta Y_L = \frac{1}{j\omega L_{\rho_o}^{ext} + Z_{\rho_o}^{int}} - \frac{1}{j\omega L_{\rho_o}^{ext^o}}. \quad (11)$$

The terms $\Delta Y_C$ and $\Delta Y_L$ represent the excess capacitance and inductance per-unit-length of the slot due to wall losses and the presence of a lossy gasket not taken into account by the equivalent antenna radius $a$. Table I gives a summary of the terms included in $\Delta Y_C$ and $\Delta Y_L$.

We now want to add a shielded enclosure in the unilluminated region. Consider the cavity-backed narrow slot aperture shown in Fig. 4 with a plane wave impinging from the left half-space $x < 0$. The first term in (3) represents the total field on the unilluminated, or cavity side. In the half-space case, this term is combined with the scattered field expression on the illuminated side since the Green's function is the same for both regions. Removal of the $\rho_o$ dependence in the half-space case was achieved by expanding the integral for the scattered field and canceling terms of the local transmission-line parameters $Z_{\rho_o}$ and $Y_{\rho_o}$ of the equivalent magnetic antenna of radius $a$. With an enclosure, the same approach is taken except that the field on the unilluminated side will be written as a sum of a half-space scattered field identical to that used in the pure half-space case and a difference field

$$H_z^+(\rho_o, z) = H_z^{HS}(\rho_o, z) + \Delta H_z(\rho_o, z) \quad (12)$$

$$= -H_z^-(\rho_o, z) + \Delta H_z(\rho_o, z) \quad (13)$$

where as before

$$H_z^{HS}(\rho_o, z) = \left[ \left( \frac{j}{\omega \mu_o} \right) \left( \frac{d^2}{dz^2} + k^2 \right) \right] \int_{-h}^{h} I_m(z') \frac{e^{-jkR_o}}{4\pi R_o} dz'$$
$$= -H_z^-(\rho_o, z). \quad (14)$$

TABLE I
GASKET AND SLOT PARAMETERS

| Quantity | Description |
|---|---|
| $G$ | Accounts for losses in the gasket material in the interior of the slot |
| $C_{\rho_o}^o$ | Local external* capacitance per-unit-length without the gasket present (walls may have finite conductivity) |
| $C_{\rho_o}$ | Local external* capacitance per-unit-length with the gasket present (walls may have finite conductivity) |
| $L_{\rho_o}^{ext^o}$ | Local external* inductance per-unit-length without the gasket present (assuming perfectly conducting walls) |
| $L_{\rho_o}^{ext}$ | Local external* inductance per-unit-length with the gasket present (assuming perfectly conducting walls) |
| $Z_{\rho_o}^{int}$ | Internal impedance per-unit-length which accounts for losses within the walls and includes changes in the inductance due to variations of the magnetic field outside the walls due to finite internal** conductivity |
| | * External to the conducting walls |
| | ** Internal to the conducting walls |
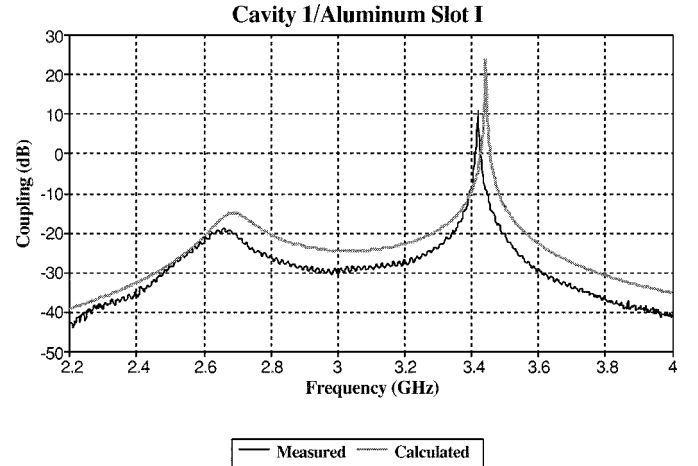


Fig. 4. Narrow-slot aperture with depth.

Therefore, the governing integral equation becomes

$$-\Delta H_z(\rho_o, z) + \left[ 2H_z^-(\rho_o, z) + \frac{1}{2Z_{\rho_o}} \frac{d^2 I_m}{dz^2} - Y_{\rho_o} \frac{I_m}{2} \right] = -H_z^{SC}(z). \quad (15)$$

If we use the procedure of Warne and Chen, the $\rho_o$ dependence in the second term of (15) is eliminated yielding

$$-\Delta H_z(\rho_o, z) + 2H_z^-(a, z) + \frac{\Delta Y_L}{2} \frac{d^2 I_m(z)}{dz^2} - \frac{\Delta Y_C}{2} I_m(z) = -H_z^{SC}. \quad (16)$$

Note that the difference field is still dependent on the arbitrary distance parameter, $\rho_o$.

For the unilluminated side, the governing equation is the vector wave equation

$$\nabla \times \frac{1}{\epsilon_r} \nabla \times \overline{H}^+ - \mu_r k_o^2 \overline{H}^+ = -\overline{M} \qquad (17)$$

where the $\hat{z}$ component of $\overline{H}^+$ is given by (12). To solve the slot/cavity coupling problem, we determine the $z$ component of the difference field at a radius $\rho_o$ from the aperture wall. This is accomplished by either: 1) solving (16), with $\overline{M}$ specified in terms of $I_m$, and subtracting the half-space field or 2) computing the difference field directly. In either case, the boundary conditions on the *total field* must be enforced. At the surface of a perfect electric conductor we have

$$\hat{n}_c \times \nabla \times \overline{H}^+ = 0 \qquad (18)$$

where the unit normal points outward from the cavity volume. At the surface of a good conductor, we relate the electric and magnetic field via the surface impedance

$$\overline{E}_{\text{tan}}^+ = Z_s \left( \hat{n}_w \times \overline{H}^+ \right) \qquad (19)$$

or more conveniently as

$$\hat{n}_c \times \nabla \times \overline{H}^+ = j\omega\epsilon Z_s \hat{n}_c \times \hat{n}_w \times \overline{H}^+ \qquad (20)$$

where $\hat{n}_w$ points from the conducting wall into the cavity volume.

Solution of (17) is simpler in terms of enforcing the boundary conditions, but involves added complication because the equivalent magnetic current $\overline{M}$ must "drive" the cavity. Although possible, this can lead to numerical problems because the mesh density must be fine enough to adequately represent the magnetic current along the slot. This somewhat defeats the purpose of using the local transmission-line model. Here, we take the second approach and solve for the difference field directly. Instead of a forced problem we solve the homogeneous wave equation with $\overline{M} = 0$

$$\nabla \times \frac{1}{\epsilon_r} \nabla \times \overline{H}^+ - \mu_r k_o^2 \overline{H}^+ = 0. \qquad (21)$$

Since the half-space field $\overline{H}^{HS}$ is a solution of the homogeneous wave equation, we obtain the following result upon substitution of (12) into (21):

$$\nabla \times \frac{1}{\epsilon_r} \nabla \times \Delta\overline{H} - \mu_r k_o^2 \Delta\overline{H} = 0. \qquad (22)$$

The forcing function for this problem becomes the incident half-space field via (12) and (20).

## III. HYBRID NUMERICAL MODEL

Here, we discuss the numerical solution of the governing equations previously formulated. We shall first discuss the discretization of the integral (16). Then the FEM solution of the 3-D vector wave equation is given. The hybrid technique utilized in the solution of slot/cavity problems will then be presented.
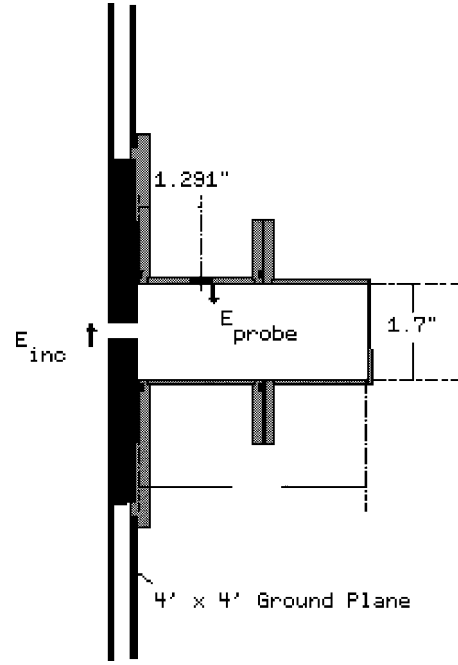


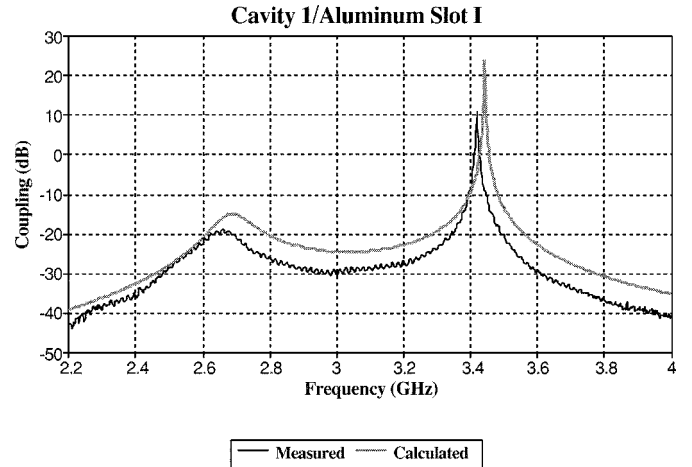Fig. 5. Cavity fixture and probe location.



Fig. 6. Coupling versus frequency for cavity 1/aluminum slot I.

### A. Method of Moments

The unknown is the equivalent magnetic current $I_m$. Just as in the thin-wire dipole problem, it is convenient to utilize piecewise sinusoids. The magnetic current is approximated by

$$\tilde{I}_m = \sum_{n=1}^{N_{\text{slot}}} A_n b_n(z) \qquad (23)$$

where $A_n$ is a complex constant to be determined and $b_n(z)$ are the piecewise sinusoidals. Each basis function is described mathematically as

$$b_n(z) = \begin{cases} \dfrac{\sin\left[k\left((z_n - z) + \Delta z\right)\right]}{\sin[k\Delta z]} & \forall z_n \leq z \leq z_n + 1 \\[3mm] \dfrac{\sin\left[k\left((z - z_n) + \Delta z\right)\right]}{\sin[k\Delta z]} & \forall z_{n-1} \leq z \leq z_n \\[3mm] 0, & \text{otherwise} \end{cases} \qquad (24)$$

where

$$\Delta z = z_{n+1} - z_n \, \forall \, n = 1, 2, \cdots, N_{\text{slot}}$$
$$\Delta z = z_n - z_{n-1} \, \forall \, n = 1, 2, \cdots, N_{\text{slot}}. \quad (25)$$

Using the Galerkin method to discretize (16) yields the $N \times N$ system of equations

$$[[Y_C] + [TY_L^C] - [TY_C^C] - [C^C]] \{A\} = -\{f_i^C\} \quad (26)$$

where the entries for each matrix are

$$Y_{in}^C = \frac{-j}{2\pi\omega\mu_o} \int_{z_m-\Delta z}^{z_m+\Delta z} b_i(z)$$
$$\cdot \left( \frac{d^2}{dz^2} + k^2 \right) \int_{z_n-\Delta z}^{z_n+\Delta z} b_n(z') \frac{e^{jkR_a}}{R_a} \, dz' \, dz \quad (27)$$

$$TY_{L_{in}}^C = \frac{\Delta Y_L}{2} \int_{z_m-\Delta z}^{z_m+\Delta z} b_i(z) \left( \frac{d^2}{dz^2} b_n(z) \right) \, dz \quad (28)$$

$$TY_{C_{in}}^C = \frac{\Delta Y_C}{2} \int_{z_m-\Delta z}^{z_m+\Delta z} b_i(z) b_n(z) \, dz \quad (29)$$

$$f_i^C = \int_{z_m-\Delta z}^{z_m+\Delta z} b_i(z) H_z^{SC} \, dz \quad (30)$$

$$C_{in}^C = \int_{z_m-\Delta z}^{z_m+\Delta z} b_i(z) \Delta \tilde{H}_z(\rho_o, z) \, dz. \quad (31)$$

Note that there are two unknowns in (26): the coefficients, $A_n$ of the slot magnetic current and the difference field $\Delta \tilde{H}_z(\rho_o, z)$. The next section will discuss the numerical formulation for the unknown cavity difference field.

### B. Finite-Element Discretization

The FEM is chosen so that irregularly shaped cavities containing highly inhomogeneous materials can be modeled. Due to the finite-element representations selected, the shapes are limited by bounding surfaces that can be approximated by second-order polynomial functions. In addition, the implementation allows varying dielectrics to be placed within the cavity as long as each finite element of the geometric mesh contains a homogeneous medium. As with many real cavities, the $Q$ of the systems modeled, as well as measured, in this investigation are in many cases rather large. As has often been encountered in the 3-D finite-element modeling of electromagnetic systems, spurious modes may result from the choice of basis functions and their numerical implementation [32]. These are simply artifacts of the numerical implementation and are nonphysical. To overcome these problems, this investigation utilized the mixed-order elements of Crowley [33]. These are similar in form to the edge-based functions used by others but, as implemented here, are nodal-based.
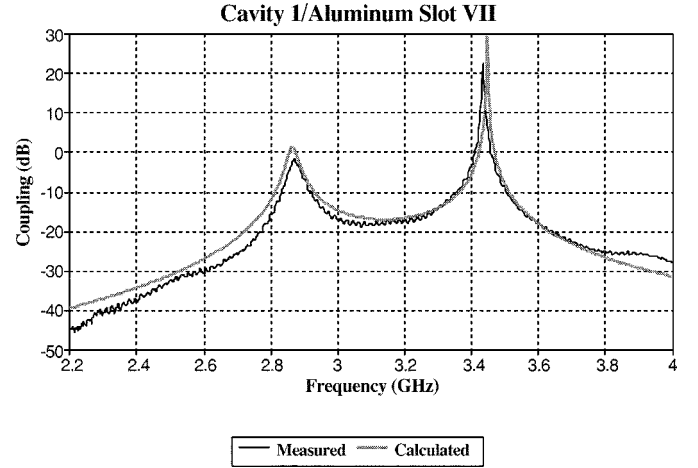


Fig. 7. Coupling versus frequency for cavity 1/aluminum slot VII.

We begin by testing (22) with a set of testing or weighting functions as yet unspecified to obtain the weak form of the vector wave equation

$$\iiint_{V^c} \overline{T}_p \cdot \left[ \nabla \times \frac{1}{\epsilon_r} \nabla \times \Delta\overline{H} - \mu_r k_o^2 \Delta\overline{H} \right] \, dV = 0, \quad \forall p. \quad (32)$$

The index on the set of independent weighting functions varies as $p = 1, 2, \cdots, N_{FEM}$. $N_{FEM}$ is the number of unknowns in the finite-element problem. $\Delta\overline{H}$ is the desired field quantity for which we wish to find an approximate solution. It is a function of the unknown magnetic current along the slot, $I_m(z)$. Using Green's theorem (32) can be rewritten as

$$\iiint_{V^c} (\nabla \times \overline{T}_p) \cdot \left( \frac{1}{\epsilon_r} \nabla \times \Delta\overline{H} \right) - \mu_r k_o^2 \overline{T}_p \cdot \Delta\overline{H} \, dV$$
$$+ \iint_{S^c} \overline{T}_p \cdot \hat{n}_c \times \left( \frac{1}{\epsilon_r} \nabla \times \Delta\overline{H} \right) \, dS = 0, \quad \forall p. \quad (33)$$

A major contributor to the reduction of $Q$ in most cavities is wall loss which must be included in our model. For a good, but not perfect, conductor we substitute the expression for the total field, the vector form of (12), into (20) and use Maxwell's equation from Ampere's law to find

$$\iiint_{V^c} (\nabla \times \overline{T}_p) \cdot \left( \frac{1}{\epsilon_r} \nabla \times \Delta\overline{H} \right) - \mu_r k_o^2 \overline{T}_p \cdot \Delta\overline{H} \, dV$$
$$+ \iint_{S^c} \overline{T}_p \cdot \hat{n}_c \times \hat{n}_w \times j\omega\epsilon_o Z_s \Delta\overline{H} \, dS$$
$$= - \iint_{S^c} \overline{T}_p \cdot \hat{n}_c \times \hat{n}_w \times j\omega\epsilon_o Z_s \overline{H}^{HS} \, dS$$
$$+ \iint_{S^c} \overline{T}_p \cdot \hat{n}_c \times j\omega\epsilon_o \overline{E}^{HS} \, dS, \quad \forall p. \quad (34)$$

Note that in the case of perfectly conducting walls, the surface impedance approaches zero $Z_s \rightarrow 0$ and we obtain (33).

Now we address the implementation of the FEM used to compute the solution. We wish to find an approximation to $\Delta\overline{H}$, call
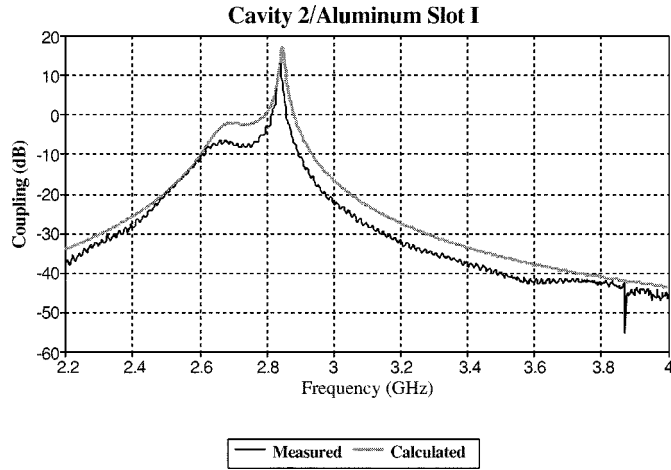
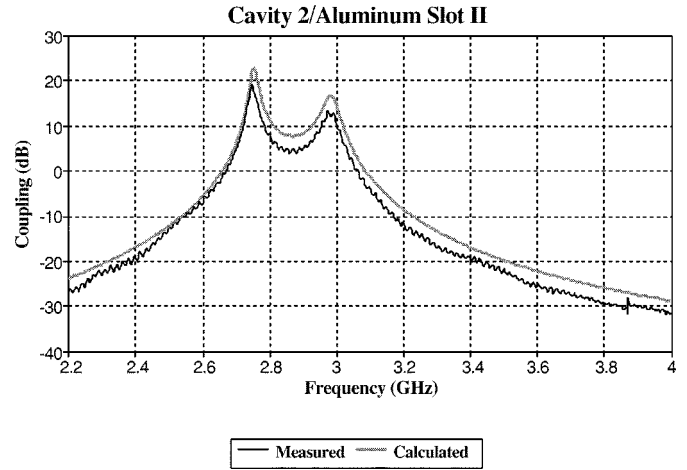Fig. 8.   Coupling versus frequency for cavity 2/aluminum slot I.



Fig. 9.   Coupling versus frequency for cavity 2/aluminum slot II.

it $\Delta\overline{\overline{H}}$. Discretizing the domain into finite elements, where the elements are assumed to be homogeneous, (34) becomes

$$
\sum_{e=1}^{N_{elem}} \left[ \frac{1}{\epsilon_r} \iiint_{V^e} \left( \nabla \times \overline{T}_p \right) \cdot \left( \nabla \times \Delta\overline{\overline{H}} \right) - \mu_r k_o^2 \overline{T}_p \right.
$$

$$
\left. \cdot \Delta\overline{\overline{H}}\overline{H}\, dV + \iint_{S^e} \overline{T}_p \cdot \hat{n}_c \times \hat{n}_w \times j\omega\epsilon_o Z_s \overline{\overline{H}} \Delta \overline{H}\, dS \right]
$$

$$
= \sum_{e=1}^{N_{elem}} \left[ -\iint_{S^e} \overline{T}_p \cdot \hat{n}_c \times \hat{n}_w \times j\omega\epsilon_o Z_s \overline{H}^{HS}\, dS \right.
$$

$$
\left. + \iint_{S^e} \overline{T}_p \cdot \hat{n}_c \times j\omega\epsilon_o \overline{E}^{HS}\, dS \right], \quad \forall p. \tag{35}
$$

The finite-element discretization of Crowley is used here. The finite elements are hexahedral, with the vector basis being a set of 54 different polynomial functions, which, for each scalar direction, utilize a set of eighteen independent shape functions; that is, there are $N_e = 18$ unknowns per component for each finite element subdomain. In compact matrix notation, (35) on a term-by-term basis becomes

$$
\sum_{e=1}^{N_{elem}} \left[ \frac{1}{\epsilon_{re}}[GM_{1e}] - \mu_{re}k_o^2[GM_{2e}] + j\omega\epsilon_o Z_{se}[GM_{3e}] \right] \left\{ \overline{\overline{H}}\Delta \right\}
$$

$$
= \sum_{e=1}^{N_{elem}} \left\{ j\omega Z_{se}\{g_{1e}\} + j\omega\epsilon_o\{g_{2e}\} \right\}. \tag{36}
$$

Note that the boundary terms cancel for internal elemental surfaces so that the elemental matrices, $[GM_{3e}]$, $\{g_{1e}\}$, and $\{g_{2e}\}$ must only be evaluated for elements bordering a conductor. The terms $\{g_{1e}\}$ and $\{g_{2e}\}$ are vectors computed from the half-space fields due to the slot magnetic currents, $I_m$. The elemental integrations are performed use Gauss–Legendre quadrature.

For a swept-frequency response calculation, the elemental assemblies for $[GM_{1e}]$, $[GM_{2e}]$, and $[GM_{3e}]$ are done once; the global matrix at each frequency is reconstructed by updating
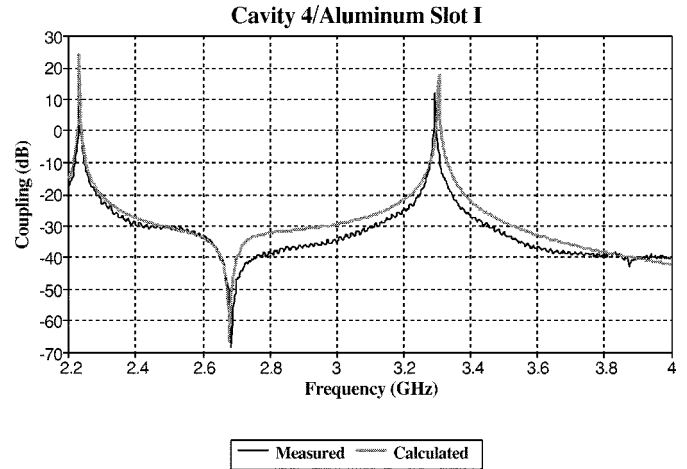


Fig. 10.   Coupling versus frequency for cavity 4/aluminum slot I.
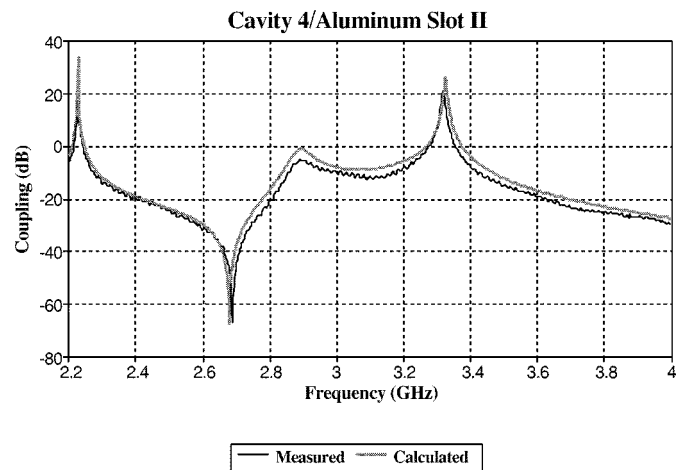


Fig. 11.   Coupling versus frequency for cavity 4/aluminum slot II.

the multipliers; and, finally, the right-hand side terms which are explicitly a function of frequency, are recomputed. This saves considerable computational time. Thus, given a presumed slot current distribution, which produces $\overline{H}^{HS}$ and $\overline{E}^{HS}$, we can solve to find the interior cavity fields.

## C. Hybrid Solution

The hybrid moment method/FEM solution to find the magnetic current along the cavity-backed slot is now presented. Equations (26) and (36) together are a set of algebraic equations to solve for the unknown slot magnetic currents and cavity difference fields. These can be solved either simultaneously or in a two-step process. We have chosen to utilize the latter to avoid the problems of having to deal with a sparse matrix having a block-dense portion.

In the two-step process, the cavity is excited at each frequency by the half-space fields $N_{\text{slot}}$ times; that is, we compute $\overline{E}^{HS}$ and $\overline{H}^{HS}$ due to each MOM slot basis function and determine $\Delta \tilde{H}_z$. While the values from the FEM solution are available, we compute a column of the $[C^C]$ matrix by testing the fields resulting from each MOM basis excitation. Solving the FEM problem $N_{\text{slot}}$ times yields the complete $N_{\text{slot}} \times N_{\text{slot}}$ matrix and the MOM problem solution can proceed. As implemented here, after the solution is completed, the $[C^C]$ matrix is stored on disk. It is then read and the MOM problem is solved via (26). At this juncture, we must also save the FEM and half-space fields ($\Delta \tilde{H}$ and $H^{HS}$) due to excitation by each MOM basis at the measurement point within the cavity. If the fields everywhere in the interior region are desired, it is necessary to store the half-space and difference fields at every node within the finite-element mesh for each excitation. In this study, we are interested in comparison to laboratory measurements performed at a single probe location; thus, only the fields at the measurement point are required.

Once the vector of magnetic current amplitudes $\{A\}$ is known, the magnetic current distribution along the slot is determined. The fields scattered by the cavity-backed aperture can then be computed by substituting $\{A\}$ into (23) and then using (9). The total cavity fields in local coordinates at the measurement point are then computed as

$$\tilde{H}_s^+ = \sum_{n=1}^{N_{\text{slot}}} A_n \left( H_{s_n}^{HS} + \Delta \tilde{H}_{s_n} \right) \tag{37}$$

$$\tilde{H}_t^+ = \sum_{n=1}^{N_{\text{slot}}} A_n \left( H_{t_n}^{HS} + \Delta \tilde{H}_{t_n} \right) \tag{38}$$

$$\tilde{H}_u^+ = \sum_{n=1}^{N_{\text{slot}}} A_n \left( H_{u_n}^{HS} + \Delta \tilde{H}_{u_n} \right). \tag{39}$$

Note that a transformation of these fields must be done to find the fields in the global Cartesian coordinate system. The electric field can be calculated from the computed values of $\overline{H}^{HS}$ and $\Delta \tilde{H}$. Given the finite element within the mesh and the position within that subdomain, we numerically take the curl of the magnetic field to find the electric field.

It should be noted that the computation of $[C^C]$ in (26) is dependent on the radius parameter $\rho_o$. It would seem that the antenna radius would greatly affect the energy stored in the vicinity of the slot; however, we wish to determine $\Delta H_z(\rho_o, z)$ rather than the half-space field in the nonlocal region. In order to
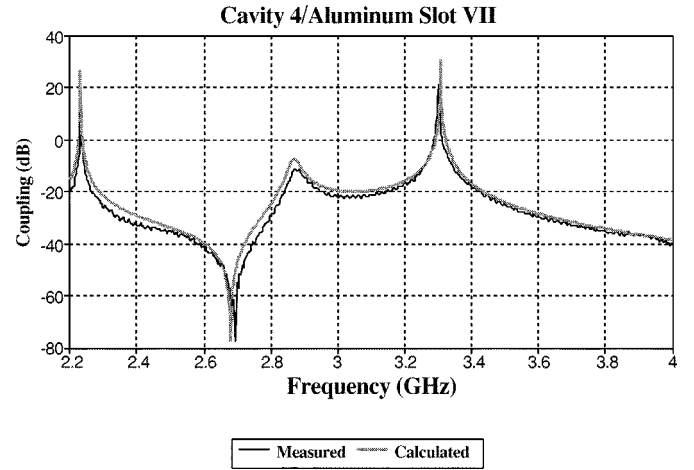


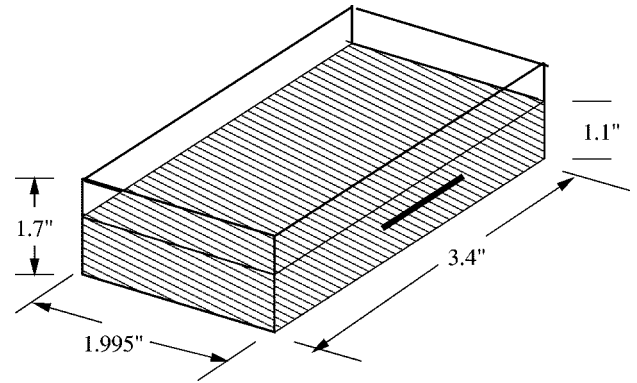Fig. 12.    Coupling versus frequency for cavity 4/aluminum slot VII.

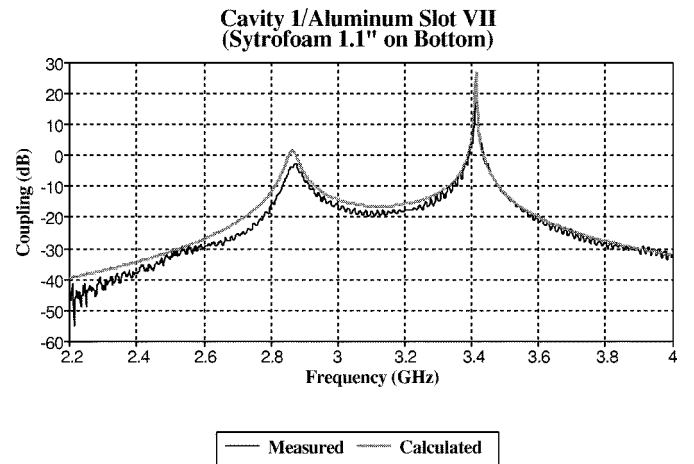

Fig. 13.    Styrofoam on bottom.



Fig. 14.    Cavity 1/aluminum slot VII (styrofoam on bottom).

cancel the $\rho_o$ dependence of the local transmission-line terms, it was necessary to evaluate the half-space field in the plus region at $\rho = a$, the equivalent antenna radius. The question then becomes "what is the dependence of the $z$-component of the difference field near the conducting wall?" We know that for a perfectly conducting wall the total tangential magnetic field doubles. From resonant cavity theory we know that the field in this region is relatively slowly varying. Rigorously satisfying the constraints in (1), we know that $\rho_o$ should be greater than the

slot cross-sectional dimension. However, since the half-space term evaluated at the equivalent radius accounts for most of the slot physics and the difference field does not vary radically in the region near the slot, we will evaluate the difference term on the slot wall, $x = +d/2$. The following results will show this to be a good choice for $\rho_o$.

## IV. RESULTS

A large number of experiments were performed to verify that the numerical slot-cavity model would produce accurate results. For the sake of brevity, we present some select cases. Full results can be found in [31]. All measurements were done in the anechoic chamber located in the Electromagnetics Laboratory, New Mexico State University, Las Cruces. The measurements presented were done with electric field probes fabricated and calibrated in the Electromagnetics Laboratory. The details of the measurement setup can be found in [31]. Four different cavities and seven different slots were constructed so that the effects of slot width and depth as well as cavity size could be examined. All the slots and cavities were constructed from aluminum. Tables II and III give the dimensions of each of the seven slots and four cavities used.

The slots were mounted to the front of the cavity test fixture as shown in Fig. 5. For all cases, the incident electric field is polarized perpendicular to the slot. Due to the limited size of the cavity and to preclude undesired loading only one probe was used. A measured value of $\sigma = 2.6 \times 10^7$ for the aluminum conductivity was used for all the computer models. In all cases, an effective slot length, as determined by comparison to half-space measurements, was used to compensate for the loading produced by imperfect short circuits at the slot ends.

The first set of results are for cavity 1. The first cavity resonant frequency ($TE_{101}$) is well above the slot resonance for cavity 1. The computer model used a 28 element finite-element mesh with 21 moment-method basis functions for the slot. Figs. 6 and 7 show the coupling for cavity 1, slots I, II, III, and VII, respectively. The reader should note the following characteristics in each of the plots: 1) cavity resonance frequency; 2) slot resonance frequency; 3) cavity resonance $Q$; 4) slot resonance $Q$; and 5) peak coupling. In each of the cases, the computer model correctly tracks the experimental results. As expected, the $Q$ decreases with increasing slot width. The peak coupling also increases with increasing slot width. Increasing the slot depth decreases the coupling due to wall losses. It is interesting to note that the slot greatly affects the coupling at the resonant frequency of the cavity even when the slot and cavity frequencies are widely spaced.

The second set of results are for cavity 2. The slot and cavity resonant frequencies are nearly coincident for this case. The computer model used a 35-element finite-element mesh with 21 moment-method basis functions for the slot. Figs. 8 and 9 show the coupling for cavity 2, slots I, and II, respectively. In both cases, the computer model is calculating the complex interaction of the slot and cavity. The proximity in frequency of the two resonances reduces the $Q$ of the system as a whole.

The third set of results are for cavity 4. The slot resonant frequency lies between the first two cavity resonant frequen-

TABLE II
MEASURED ALUMINUM SLOT DIMENSIONS

| Slot | Width | Depth | $l_{slot}$ | $l_{eff}$ |
|------|-------|-------|-----------|-----------|
| I | .0017" | .125" | 2.004" | 2.150" |
| II | .010" | .125" | 1.995" | 2.020" |
| III | .125" | .125" | 1.996" | 2.000" |
| IV | .0021" | .25" | 1.995" | 2.110" |
| V | .010" | .25" | 2.005" | 2.060" |
| VI | .0016" | .50" | 2.003" | 2.180" |
| VII | .0095" | .50" | 2.008" | 2.045" |

TABLE III
CAVITY DIMENSIONS

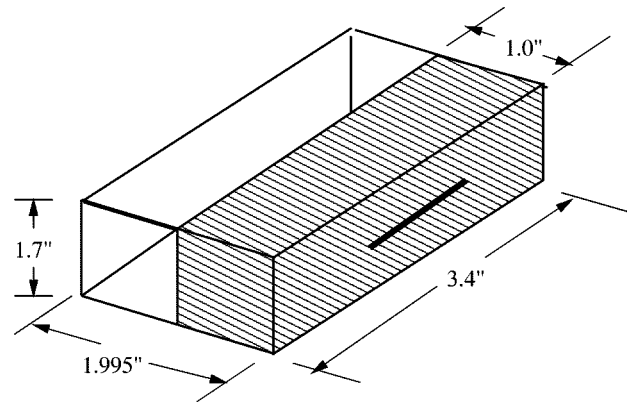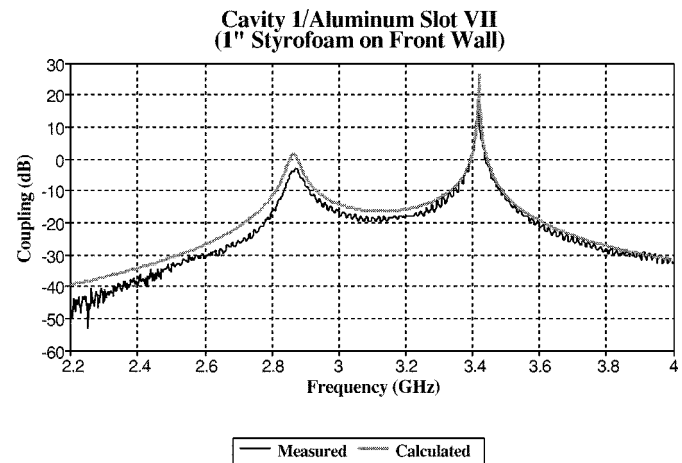| Cavity | Width | Height | Depth ($d_c$) |
|--------|-------|--------|---------------|
| 1 | 3.4" | 1.7" | 1.995" |
| 2 | 3.4" | 1.7" | 2.637" |
| 3 | 3.4" | 1.7" | 3.295" |
| 4 | 3.4" | 1.7" | 4.205" |



Fig. 15.   Styrofoam on front wall.



Fig. 16.   Cavity 1/aluminum slot VII (styrofoam on front wall).

cies. The computer model used a 63-element finite-element mesh with 21 moment-method basis functions for the slot. Figs. 10–12 show the coupling for cavity 4, slots I, II, and VII, respectively. Again, the computer model is able to predict the coupling accurately.

We now consider the effects of loading the cavity with dielectrics and conductors. The first combination is for cavity 1
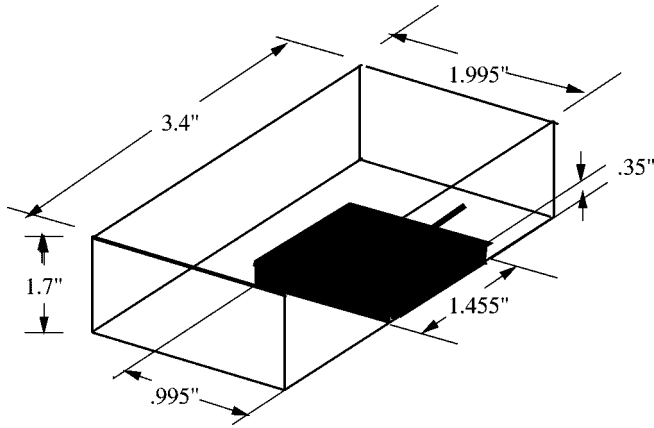
Fig. 17.   Teflon block near front wall.



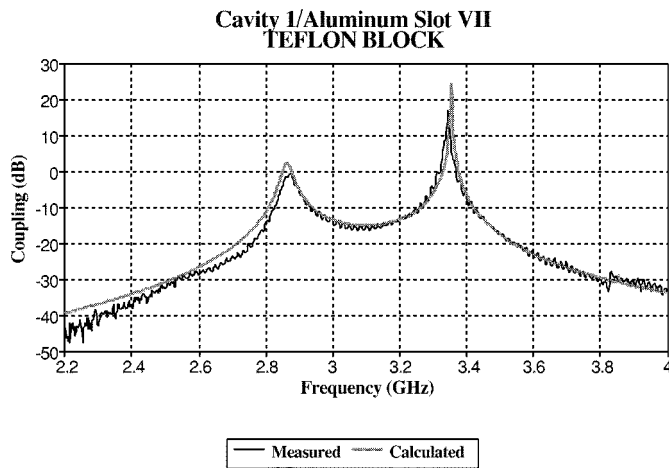Fig. 19.   Metal block on bottom wall.



Fig. 18.   Cavity 1/aluminum slot VII (teflon block near front wall).

partially filled with styrofoam with slot VII, as given in Fig. 13. The calculated and measured curves shown in Fig. 14 display excellent agreement. The measured cavity resonance decreases to 3.415 GHz. Ignoring losses, a volumetric mixing model results in $\epsilon_{r\text{eff}} = 1.018$. This results in a cavity resonant frequency decrease of 29.5 MHz, from 3.4465–3.418 GHz. The numerical model with 42 elements and 21-slot moment-method basis functions predicts a decrease of 31.5 MHz.

The second combination is for cavity 1 partially filled with styrofoam with slot VII as given in Fig. 15. The calculated and measured curves shown in Fig. 16 display excellent agreement. The measured cavity resonance decreases to 3.417 GHz. Ignoring losses, a volumetric mixing model results in $\epsilon_{r\text{eff}} = 1.017$. This results in a cavity resonant frequency decrease of 28.5 MHz, from 3.4465 to 3.418 GHz. The numerical model with 42 elements and 21-slot moment-method basis functions predicts a decrease of 27.5 MHz.

For each of the last two results, we were able to use perturbation theory to predict the cavity resonant frequency shift since the slot was narrow and has a large depth so that the cavity fields are not perturbed significantly. The agreement with the hybrid numerical technique was good although it should be pointed out that predicted shifts are about 10 MHz greater than those measured in the laboratory.
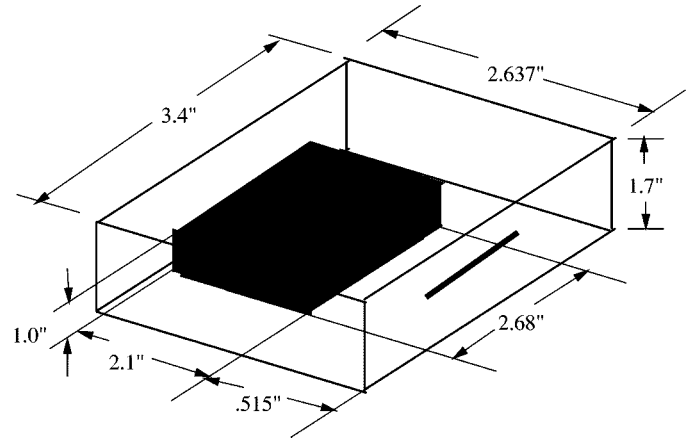
The third combination is cavity 1 with slot VII having a small teflon block placed near the front wall (Fig. 17). The published value used in the computer model was $\epsilon_r = 2.1 - j0.0003$. The frequency response curves calculated by the computer model again agree well with the measured results (Fig. 18). The measured peak shifted from 3.435 GHz in the air-filled cavity to 3.345 GHz when the dielectric slab was inserted, a downward shift of 90 MHz. Perturbation theory can be used to predict the resonant frequency shift assuming that the dielectric occlusion in the cavity is small. The shift is given as

$$\Delta f = f_{res_{\text{air}}} \frac{\Delta W}{W} \qquad (40)$$

where $\Delta W$ is the additional energy stored in the cavity with the dielectric in place, and $W$ is the energy stored without the dielectric. The shift computed with perturbation theory is 35.8 MHz. The computer model (84 elements and 21-slot moment-method basis functions) predicted a resonant frequency of 3.408 GHz which is close agreement with the shift predicted by perturbation theory. The larger measured resonant frequency shift may be indicative of an error in the measured location of the dielectric slab. A shift toward the center of the cavity more than doubles the predicted shift by either method.

The final result is for cavity 2 with slot VII having a metal block set on the lower surface of the cavity (Fig. 19). The block was not held in place with screws or bolts. It was set in the cavity so that a small gap between the block and rear wall of the cavity was created. The measured and calculated curves are shown in Fig. 20. The computer model used 100 elements and 21 slot moment method basis functions. The FEM model ignored any air gaps between the metal block and the bottom plate of the cavity. Two main features of the response are observed. First, there is a dramatic decrease in the cavity resonant frequency. The cavity resonant frequency shifts downward nearly 800 MHz to 2 GHz when the metal block is introduced. A second resonant peak of the loaded cavity is observed near 3.5 GHz. The coupling in the vicinity of the slot resonant frequency. approximately 2.8 GHz, is perturbed by the presence of the conducting block.

Although not as close as previous examples, the agreement between the computed and experimental results is still adequate for practical situations. Most importantly the hybrid

**Cavity 2/Aluminum Slot VII
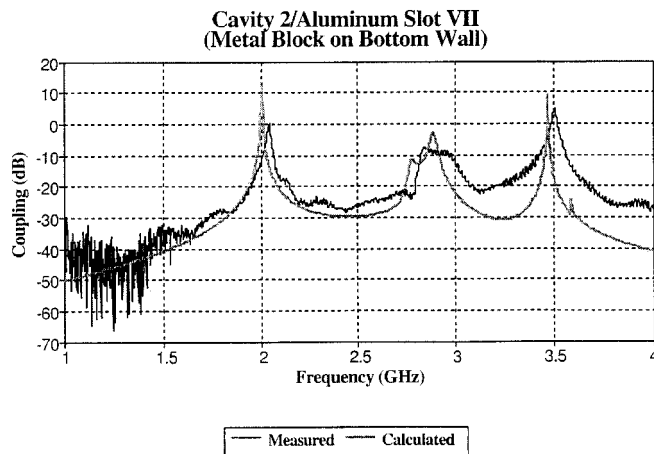(Metal Block on Bottom Wall)**



Fig. 20   Cavity 2/aluminum slot VII (metal block on front wall).

MOM/FEM model predicts the general vicinity of the two cavity peaks. These are the points in the frequency spectrum where maximum coupling occurs. Thus, in terms of determining system susceptibility, the numerical model performs well. Furthermore, the computed curve displays trends similar to those measured in the laboratory near the slot peak.

Reasons for the weaker relationship between modeled and measured data are difficult to determine in this last case. Imprecise knowledge of the dimensions of the cavity, irregularities in the dimensions of the metal block, uncertainties in its location and air gaps may have all contributed to the discrepancies.

## V. Conclusions

The primary focus of this research was the formulation and numerical solution of slot/cavity problems incorporating realistic apertures. This was accomplished by modification of the antenna/local transmission-line model of Warne and Chen, which represents the physical attributes of an actual seam by incorporating slot depth and losses, and applying it to arbitrarily-shaped cavity-backed apertures. A hybrid MOM/FEM technique was applied to solve the two-region problem utilizing standard piecewise-sinusoidal basis functions for the moment method implementation and mixed-order, covariant projection finite elements. The hybrid model was used successfully to compute the electromagnetic coupling into a variety of slot/cavity geometric configurations with varying dielectric inhomogeneities.

A series of numerical and laboratory experiments for slot/cavity configurations with right-rectangular geometries was performed, with excellent agreement between the experimental data and numerical computations. Inconsistencies were mainly attributed to loss mechanisms not represented in the hybrid MOM/FEM slot/cavity model, caused by uncertainties in the mechanical configuration. However, the model successfully indicated the relative position of slot and cavity resonances, demonstrating the interaction between the slot and the highly reactive cavity load and the resulting enhancement in coupling. The cavity fields increased with increasing slot width and/or decreased slot depth. Frequency shifts measured when the right-rectangular cavities were partially loaded with dielectric materials were predicted with the hybrid MOM/FEM model and found to be in good agreement with the results of a perturbational analysis.

The hybrid technique developed here utilizes an FEM solution of the interior cavity problem and allows for arbitrarily shaped geometries. An irregular cavity was assembled and coupling measurements performed. The hybrid MOM/FEM model predicted the nominal frequencies at which high coupling levels occurred. Although wall losses were included, the hybrid MOM/FEM model somewhat overestimated the peak coupling values, thus providing a conservative estimate of the maximum field within the cavity. That is, the measured fields in the cavity were smaller, the internal electromagnetic environment was less severe than that predicted by the hybrid MOM/FEM model.

The mixed-order covariant-projection finite elements described by Crowley allow curvilinear geometries to be accurately modeled with a minimum number of elements. The use of the slot model of Warne and Chen avoids the need for using a fine discretization in the slot region further adding to the efficiency of the method.

An additional advantage of the hybrid numerical model used here is that in the course of computing the coupling, the fields everywhere within the cavity can be determined. For a given configuration, this ensures that the maximum field and its location are determined. This is often difficult to accomplish in a measurement program. Furthermore, the numerical analysis allows determination of the energy distribution within the system.

To enhance the capabilities of the slot/cavity formulation presented here, realism should be added to the exterior problem and terminated wires as well as complex loads should be included within the interior cavity region.

## References

[1] R. F. Harrington and J. R. Mautz, "A generalized network formulation for aperture problems," *IEEE Trans. Antennas Propagat.*, vol. AP-24, pp. 870–873, Nov. 1976.

[2] C. M. Butler, Y. Ramat-Samii, and R. Mittra, "Electromagnetic penetration through apertures in conducting screens," *IEEE Trans. Antennas Propagat.*, vol. AP-26, pp. 82–93, Jan. 1978.

[3] R. F. Harrington, *Field Computation by Moment Methods.*   New York: Cazenovia, 1968.

[4] T. Wang, R. F. Harrington, and J. R. Mautz, "Electromagnetic scattering from and transmission through arbitrary apertures in conducting bodies," *IEEE Trans. Antennas Propagat.*, vol. 38, pp. 1805–1814, Nov. 1990.

[5] A. Taflove, K. R. Umashankar, B. Beker, F. Harfoush, and K. S. Yee, "Detailed FD-TD analysis of electromagnetic fields penetrating narrow slots and lapped joints in thick conducting screens," *IEEE Trans. Antennas Propagat.*, vol. 36, pp. 247–257, Feb. 1988.

[6] D. E. Merewether and R. Fisher, "Finite-difference analysis of EM fields inside complex cavities driven by large apertures," *IEEE Trans. Electromagn. Compat.*, vol. EMC-24, pp. 406–410, Nov. 1982.

[7] D. J. Riley and C. D. Turner, "Hybrid thin-slot algorithm for the analysis of narrow apertures in finite-difference time-domain calculations," Sandia National Laboratories, Rep. SAND89-3073, Jan. 1990.

[8] J. Gilbert and R. Holland, "Implementation of the thin-slot formalism in the finite-difference EMP code THREDH," *IEEE Trans. Nucl. Sci.*, vol. NS-28, pp. 4269–4274, Dec. 1981.

[9] D. J. Riley and C. D. Turner, "The inclusion of wall loss in electromagnetic finite-difference time-domain thin-slot algorithms," Sandia Nat. Lab., Albuquerque, NM, Rep. SAND90-2091, Sept. 1990.

[10] ——, "The VOLMAX transient electromagnetic modeling system, including sub-cell slots and wires on random nonorthogonal cells," in *14th Annu. Rev. Progress Appl. Computat. Electromagn. (ACES) Symp. Dig.*, Monterey, CA, 1998, pp. 816–824.

[11] J. M. Jin and J. L. Volakis, "TE scattering by an inhomogeneous filled aperture in a thick conducting plane," *IEEE Trans. Antennas Propagat.*, vol. 38, pp. 280–286, Aug. 1990.

[12] ——, "TM scattering by an inhomogeneous filled aperture in a thick conducting plane," in *Proc. Inst. Elect. Eng.*, vol. 137, June 1990, pp. 153–159.

[13] S. D. Gedney and R. Mittra, "Analysis of the electromagnetic scattering by thick gratings using a combined FEM/MM solution," *IEEE Trans. Antennas Propagat.*, vol. 39, pp. 1604–1615, Nov. 1991.

[14] ——, "Electromagnetic transmission through inhomogeneously filled slots in a thick conducting plane," *IEEE Trans. Electromagn. Compat.*, vol. 34, pp. 404–415, Nov. 1992.

[15] T. J. Park, S. H. Kang, and H. J. Eom, "TE scattering from a slit in a thick conducting screen: Revisited," *IEEE Trans. Antennas Propagat.*, vol. 42, pp. 112–114, Jan. 1994.

[16] S. H. Kang, H. J. Eom, and T. J. Park, "TM scattering from a slit in a thick conducting screen: Revisited," *IEEE Trans. Microwave Theory Tech.*, vol. 41, pp. 895–899, May 1993.

[17] P. M. Goggans and T. H. Shumpert, "Backscatter RCS for TE and TM excitations of dielectric filled cavity-backed apertures in two-dimensional bodies," *IEEE Trans. Electromagn. Compat.*, vol. 39, pp. 1224–1227, Aug. 1992.

[18] K. R. Demarest, "A finite difference-time domain technique for modeling narrow apertures in conducting scatters," *IEEE Trans. Antennas Propagat.*, vol. AP-35, pp. 826–831, July 1987.

[19] R. Lee and T. T. Chia, "Analysis of electromagnetic scattering from a cavity with a complex termination by means of a hybrid ray-FDTD method," *IEEE Trans. Antennas Propagat.*, vol. 41, pp. 1560–1569, Nov. 1993.

[20] J. M. Jin and J. L. Volakis, "Electromagnetic scattering by and transmission through a three-dimensional slot in a thick conducting plane," *IEEE Trans. Antennas Propagat.*, vol. 39, pp. 543–550, Apr. 1991.

[21] ——, "A finite element-boundary integral formulation for scattering by three dimensional cavity-backed apertures," *IEEE Trans. Antennas Propagat.*, vol. 39, pp. 97–104, Jan. 1991.

[22] D. S. Dixson, M. Obara, and N. Schade, "Finite-element analysis (FEA) as EMC prediction tool," *IEEE Trans. Electromagn. Compat.*, vol. 35, pp. 241–248, May 1993.

[23] R. Laroussi and G. I. Costache, "Finite-element method applied to EMC problems," *IEEE Trans. Electromagn. Compat.*, vol. 35, pp. 178–184, Feb. 1993.

[24] L. K. Warne and K. C. Chen, "Slot apertures having depth and losses described by local transmission line theory," *IEEE Trans. Electromagn. Compat.*, vol. 32, pp. 185–196, Aug. 1990.

[25] ——, "Equivalent antenna radius for narrow slot apertures having depth," *IEEE Trans. Antennas Propagat.*, vol. 37, pp. 824–834, July 1989.

[26] ——, "Relation between equivalent antenna radius and transverse line dipole moments of narrow slot apertures having depth," *IEEE Trans. Electromagn. Compat.*, vol. 30, pp. 364–370, Aug. 1988.

[27] ——, "Electromagnetic penetration of narrow slot apertures having depth,", Air Force Weapons Lab. Interaction Note, IN-464, Apr. 1988.

[28] ——, "Slot apertures having depth described by local transmission line theory,", Air Force Weapons Lab. Interaction Note, IN-467, June 1988.

[29] ——, "A simple transmission line model for narrow slot apertures having depth and loss," *IEEE Trans. Electromagn. Compat.*, vol. 34, pp. 173–182, Aug. 1992.

[30] ——, "Effective impedance of bolt loads on narrow slot apertures having depth," *J. Electromagn. Waves Applicat.*, vol. 6, no. 7, pp. 891–910, 1992.

[31] R. P. Jedlicka, "Electromagnetic coupling into complex cavities through narrow slot apertures having depth and losses," Ph.D. dissertation, Klipsch School Elect. Comput. Eng., New Mexico State Univ., Las Cruces, NM, Dec. 1995.

[32] D. R. Lynch and K. D. Paulsen, "Origin of vector parasites in numerical maxwell solutions," *IEEE Trans. Microwave Theory Tech.*, vol. 39, pp. 383–394, Mar. 1991.

[33] C. W. Crowley, P. P. Silvester, and H. Hurwitz Jr., "Covariant projection finite elements for 3d vector field problems," *IEEE Trans. Magn.*, vol. 25, pp. 397–400, Jan. 1988.

**Russell P. Jedlicka** (S'76–M'81–SM'99) received the B.S.E.E. degree from the University of Kansas, Lawrence in 1977, and the M.S.E.E. and Ph.D. degrees from New Mexico State University, Las Cruces, in 1979 and 1995, respectively.

In 1983, he joined the staff of the Electromagnetic Systems Branch of Physical Science Laboratory, New Mexico State University. He has had a joint appointment with the Klipsch School of Electrical and Computer Engineering, New Mexico State University since 1983. His research interests include microstrip antenna analysis and design, microwave measurements, and electromagnetic coupling.

Dr. Jedlicka is a member of Eta Kappa Nu and Sigma Xi.

**Steven P. Castillo** (S'85–M'86–SM'94) photograph and biography not available at the time of publication.

**Larry K. Warne** was born in Paterson, NJ, on June 23, 1954. He received the B.S.E.E. degree from Fairleigh Dickinson University, Teaneck, NJ, in 1976, and the M.S.E.E. and Ph.D. (electrical engineering) degrees from the California Institute of Technology, Pasadena, CA, in 1977 and 1984, respectively.

He has been with Sandia National Laboratories, Albuquerque, NM, since 1978, where he is currently a distinguished member of the technical staff.